Article

Ethene Epoxidation Selectivity Inhibited by Twisted Oxametallacycle: A DFT Study on Ag Surface-Oxide

Marie-Laure Bocquet, and David Loffreda

J. Am. Chem. Soc., **2005**, 127 (49), 17207-17215• DOI: 10.1021/ja051397f • Publication Date (Web): 15 November 2005

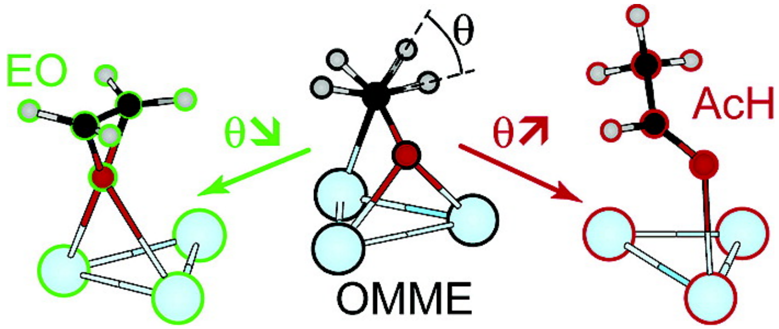

Journal of the American Chemical Society is published by the American Chemical Society. 1155 Sixteenth Street N.W., Washington, DC 20036

J|A|C|S
ARTICLES
Published on Web 11/15/2005

Ethene Epoxidation Selectivity Inhibited by Twisted Oxametallacycle: A DFT Study on Ag Surface-Oxide

Marie-Laure Bocquet* and David Loffreda

Contribution from the Laboratoire de chimie, UMR CNRS 5182, Ecole Normale Supérieure de Lyon, 46 Allée d'Italie, F-69364 Lyon, Cedex 07, France

Received March 4, 2005; E-mail: mbocquet@ens-lyon.fr

Abstract: Competitive ethene oxidation pathways are presented for a p(4 × 4) surface-oxide phase on Ag(111) obtained from density functional theory (DFT) calculations. Both parallel routes are found to proceed from a common oxametallacycle intermediate (OMME) in agreement with previous mechanistic studies on low coverage O adatom phase, although acetaldehyde (AcH) is favored by almost 2 kcal/mol. An even more striking difference with pure metal surface appears with the oxide regeneration pathways, which are found non-rate controlling. Furthermore, a kinetic model is developed on the basis of these DFT calculations and yields 96% selectivity in favor of AcH for a simulation in realistic catalytic conditions (600 K and respective partial pressures of 1 atm for ethene and oxygen reactants). As a key finding, this low ethene epoxide selectivity is proposed to be directly linked to the conformational barrier of the pivotal intermediate. In fact, the elasticity of the ultrathin oxide adlayer enables a twisted OMME structure as a true minimum, which agrees well with orbital prerequisite of the concerted H migration toward AcH. On the contrary, the desired selective ring closure forming ethene epoxide (EO) requires conformational inversion although the eclipsed form lies 2 kcal/mol above.

1. Introduction

Controlling selectivity is an essential goal in catalysis. However, fundamental factors which govern the selectivity are often misunderstood, even for ordinary reactions occurring in heterogeneous catalysis. This long-sought objective is mainly devoted to nanoscale experiments and theory since it involves the atom-by-atom structural understanding of the interface between molecules and surfaces. In computational surface science, density functional theory (DFT) has developed widely over the past decade to a point that now allows mechanistic studies with quantitative predictions of reaction barriers. To link atomistic calculations with measurable kinetic quantities, there is a call to develop related microkinetic analysis. By means of such mechanistic information, it is hoped to shed light into selective reactions to rationally design efficient catalytic materials.

The catalytic reaction chosen here is the partial oxidation of ethene by Ag to yield ethene epoxide (EO). The EO production is one of the most important industrial catalytic reactions representing a multibillion dollar worldwide process,[1] since this molecule serves as a very useful chemical intermediate from which other macroscopic materials such as plastics can be derived. Beyond these technological grounds, ethene epoxidation is also a reaction of considerable fundamental interest since it is the simplest example of a kinetically controlled catalytic oxidation. Indeed partial oxidation selectively yields the ethene epoxide as the kinetic product, although the principal byproduct is carbon dioxide, which comes from the acetaldehyde intermediate.

Industrially, the traditional catalyst uses silver particles dispersed on alumina as active component with typical selectivity ranging from 40 to 50%. The selectivity reaches 80−85% for an optimized alkali- and chlorine-promoted catalyst.[2] This intrinsic moderate selectivity represents a huge waste of valuable feedstock. However, one should keep in mind that Ag is the unique metal providing a substantial amount of epoxidation; on all other transition metals only the complete combustion proceeds.[3] Hence, solving the microscopic origin of such exceptional selectivity is of fundamental and economical interest.

Until recently, it was widely accepted that the obvious surface, which represented best unpromoted Ag catalyst under oxygenated pressure, was a chemisorbed oxygen overlayer on the characteristic (111) facet of face-centered-cubic (fcc) metals as revealed by experimental UHV studies.[4−5] On this model surface (*which we will refer to throughout the paper as "clean Ag" despite an oxygen coverage of 0.11 ML*), Linic et al. have investigated theoretically the selective reaction pathway and inferred the sequential formation of C−O bonds through the creation of a surface oxametallacycle intermediate.[6] In addition, the existence of this key intermediate has been asserted by means of classical surface techniques, such as TPD (temperature-programmed desorption) spectra, spectroscopic measurements

---

(1) *Chem. Eng. News* **2002**, June 24.

(2) Berty, J. M. Ethene Epoxide Synthesis. In *Applied Industrial Catalysis*; Leach, B. E., Ed.; Academic Press: New York, 1983; Vol. 1.

(3) Mavrikakis, M.; Doren D. J.; Barteau, M. A. *J. Phys. Chem. B* **1998**, *102*, 394.

(4) Zambelli, T.; Wintterlin J.; Trost, J.; Ertl, G. *Science* **1996**, *273*, 1688.

(5) Somorjai, G. A. *Introduction to Surface Chemistry And Catalysis*; John Wiley & Sons: New York, 1994; Somorjai, G. A. *J. Mol. Struct. (THEOCHEM)* **1998**, *424*, 101.

(6) Linic S.; Barteau, M. A. *J. Am. Chem. Soc.* **2003**, *125*, 4034.

10.1021/ja051397f CCC: $30.25 © 2005 American Chemical Society

(HREELS),[7] and HRXPS (high-resolution X-ray photoelectron spectra) surface analysis.[8]

However, as stated recently for ruthenium,[9−10] platinum,[11] and palladium,[12] transition metal surfaces are presumably no longer present under exposure of oxygen pressure in the operating catalytic reactor and exhibit a two-dimensional surface-oxide responsible for the catalytic activity.

Motivated by these observations and using the interplay between STM-UHV experiment and DFT-derived phase diagrams, we have previously predicted two O superstructures on silver catalyst to be stable under high temperature and oxidizing pressure: a low-coverage atomic phase (0.06 ML) and a defected p(4×4) oxide overlayer (ranging around 0.4 ML).[13−15] This latter high-coverage O phase actually presents Ag vacancies on low coordinated sites of the underlying Ag substrate and can be rationalized with $Ag_{1.83}O$ stoichiometry. Next, we have investigated the epoxidation mechanism on this $Ag_{1.83}O$/Ag surface and compared it quantitatively with the "clean Ag" surface.[16] Despite a different chemical environment surrounding the extractable oxygen, computed epoxidation reactions proceeded through the same two-step mechanism and displayed similar barriers. In addition, concerted mechanisms (in which O adds across the double C−C bond directly producing epoxide) have been ruled out. The subsequent similar reactivity on both catalysts accounts for the very little influence of the local substrate structure facing ethene reactant.

The first study devoted to the selectivity question on clean Ag has been published recently by Linic et al. A competing route for the destruction of the oxametallacycle has been calculated, either the C−Ag bond breaking and O abstraction for the EO, or the same bond breaking and H migration to allylic C for the acetaldehyde (AcH).[6,17] The kinetic (EO) versus thermodynamic (AcH) routes show almost equal energetic barriers at finite temperature, with a slight preference for the formation of AcH in qualitative agreement with reported selectivities ranging below 50% of ethene epoxide.

To date, the selectivity question on the (4×4) overlayer has not been tackled from DFT calculations. The first aim of the present theoretical work is to show how the oxide-like environment of Ag active sites may affect the competitive isomerization process. Herein we will present the whole catalytic cycle on the surface-oxide silver catalyst. By reporting an analogous oxidation mechanism as on clean Ag, our contribution will corroborate the growing evidence of the pivotal role played by the surface intermediate on various kinds of Ag−O chemical environment. The second aim is to yield a selectivity prediction on the basis of a microkinetic modeling, 96% selectivity in favor of acetaldehyde is thus computed that poorly compares with previous kinetic studies based on parametrized adsorption values[18−19] or similar investigations on clean Ag.[17] It is argued that this *reverse selectivity* on the surface-oxide is uniquely controlled by the *reverse* stable conformation for the surface intermediate compared to that for pure metal surfaces due to its intrinsic flexibility.

2. Methodology

2.1. Total Energy Calculations. The structure calculations are based on a DFT slab approach using the plane-wave pseudopotential code VASP[20] with the GGA-PW91 functional.[21] Vanderbilt ultrasoft pseudopotentials are used with a plane-wave cutoff energy of 400 eV.[22] The supercell approach is used to describe the Ag surface with each repeat unit containing three substrate Ag layers and an oxide trilayer O−Ag−O in a 4×4 lateral unit cell. The vacuum region above the surface is equivalent to six metallic interlayer distances to avoid unphysical image interactions between adjacent cells along the (111) direction. All reaction intermediates are adsorbed on the oxide trilayer, and simultaneous relaxations of the adsorbate, the surface-oxide, and the top layer of the bare Ag slab are performed until self-consistent forces are lower than 0.01 eV/Å. For all presented optimized states, the integration over the 4×4 surface Brillouin zone is performed by discrete summation on an irreducible set of five weighted sampling points corresponding to a ($3 \times 3 \times 1$) mesh following the Monkhorst−Pack procedure.[23] The "systematic" error[24] of the model is estimated to 20 meV by using different pseudopotential schemes (projector-augmented-wave, PAW[25]). The mean numeric error due to the convergence of total energy with k-point density is less than 15 meV. These two error bars show a negligible effect on the relative height of the activation barriers and the adsorption energies discussed hereafter.

2.2. Reaction Pathway Minimization and Frequency Analysis. A delicate issue of this computational work is the minimization of the reaction pathways and the search of the intermediate stationary points (saddle point SP) connecting the phase spaces of reactant and product. The climbing-image nudged elastic band method[26] implemented in VASP has been systematically used to find these saddle points along the minimal energy pathway (MEP) connecting each initial and final state of a given elementary step. Approximate structures of SP are obtained with the minimization of a set of eight intermediate images. To refine the SP geometry we have further minimized all the residual forces with a quasi-Newton algorithm. Finally, the key stationary points have been identified as transition states (TS) with a vibrational analysis showing the existence of a single normal mode associated with a pure imaginary frequency (as described later).

In the vibrational analysis, all degrees of freedom of the relaxed atoms are considered (Ag substrate, Ag oxide trilayer, and adsorbate). The Hessian matrix is obtained with the numerical calculation of the second derivatives of the potential energy surface built with finite differences of the atomic forces (see ref 27 for more details). Diagonalization of this force constant matrix provides the harmonic

---

(7) Linic S.; Barteau, M. A. *J. Am. Chem. Soc.* **2003**, *124*, 310.

(8) Linic, S.; Piao, H.; Adib, K.; Barteau, M. A. *Angew. Chem., Int. Ed.* **2004**, *43*, 2918.

(9) Over, H.; Kim, Y. D.; Seitsonen, A. P.; Wendt, S.; Lundgren, E.; Schmid, M.; Varga, P.; Morgante, A.; Ertl, G. *Science* **2000**, *287*, 1474.

(10) Over, H.; Seitsonen, A. P. *Science* **2002**, *297*, 2003.

(11) Hendriksen, B. L. M.; Frenken, J. W. M. *Phys. Rev. Lett.* **2002**, *89*, 046101

(12) Hendriksen, B. L. M.; Bobaru, S. C.; Frenken, J. W. M. *Surf. Sci.* **2004**, 552.

(13) Carlisle, C. I.; King, D. A.; Bocquet, M.-L.; Cerda, J.; Sautet, P. *Phys. Rev. Lett.* **2000**, *84*, 3899.

(14) Carlisle, C. I.; Fujimoto, T.; Sim, W. S.; King, D. A. *Surf. Sci.* **2000**, *470*, 15.

(15) Michaelides, A.; Bocquet, M.-L.; Sautet, P.; Alavi, A.; King, D. A. *Chem. Phys. Lett.* **2003**, *367*, 344.

(16) Bocquet, M.-L.; Michaelides, A.; Loffreda, D.; Sautet, P.; Alavi, A.; King, D. A. *J. Am. Chem. Soc.* **2003**, *125*, 5620.

(17) Linic, S.; Barteau, M. A. *J. Catal.* **2003**, *214*, 200.

(18) Stegelman, C.; Stoltze, P. *J. Catal.* **2004**, *226*, 129.

(19) Stegelman, C.; Schiodt, N. C.; Campbell, C. T.; Stoltze, P. *J. Catal.* **2004**, *221*, 630.

(20) Kresse, G.; Furthmüller, J. *Comput. Mater. Sci.* **1996**, *6*, 15; *Phys. Rev. B* **1996**, *54*, 11169.

(21) Perdew, J. P.; Wang, Y. *Phys. Rev. B* **1992**, *45*, 13244.

(22) Vanderbilt, D. *Phys. Rev. B* **1990**, *41*, R7892.

(23) Monkhorst, H. J.; Pack, J. D. *Phys. Rev. B* **1976**, *13*, 5188.

(24) The "systematic" error has been roughly estimated by comparing equivalent classes of GGA functional (PW91 and PBE) combined with different pseudopotentials (USPP PW91 and PAW PW91 and PBE), since calculations with hybrid functionals (B3LYP) or comparisons with experiments are not possible.

(25) Kresse, G.; Joubert, D. *Phys. Rev. B* **1999**, *59*, 1758.

(26) Henkelman, G.; Uberuaga, B. P.; Jonsson, H. *J. Chem. Phys.* **2000**, *113*, 9901.

(27) Loffreda, D.; Jugnet, Y.; Delbecq, F.; Bertolini, J.-C.; Sautet, P. *J. Phys. Chem. B* **2004**, *108*, 9085.

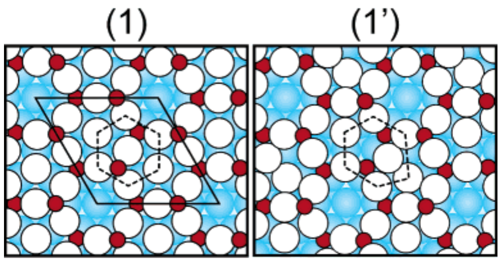

Figure 1. Top view of the bare $Ag_{1.83}O/Ag(111)$ surface (1) prior to and (1′) during ethene oxidation. The 4 × 4 lateral unit cell is indicated by the black parallelogram in (1). Constitutive atoms of the surface-oxide are depicted by large white (Ag) and small red (O) balls, while the underlying Ag substrate atoms are described by large blue balls. The considered Ag active site resides in the center of the dotted line hexagon. Hexagon apexes mark positions of the first neighboring shell of Ag atoms. Upon oxidation, the surface undergoes a marked deformation as shown in (1′): the active Ag site is shifted laterally toward a metallic Ag atom, and the O−Ag−O angle is thus bent.

frequencies (adsorbate frequencies and surface phonons only at the Γ-point) and associated harmonic normal modes.

Finally, it should be noted that the pathway minimization procedure and the vibrational frequency analysis are both performed at Γ-point for feasibility. However, all resulting states (intermediates or transition states described in the figures) result from a further geometry optimization with the finer (3 × 3 × 1) k-point grid which is stated in section 2.1.

3. Density Functional Theory Calculations

3.1. Intermediate Adsorption States: Structure, Energetics, and Vibrational Analysis.

3.1.1. Deformation of the Catalyst. Figure 1 (1) displays a top view of the surface catalyst composed of a thin slab of a trilayer Ag oxide deposited on (111) Ag substrate. The surface-oxide is formed by two layers of O atoms, respectively down and up, and one Ag layer composed of metallic and oxide-like Ag atoms. The main feature of this surface is that O−Ag−O linkages form interconnected rings and two-thirds of these rings encircle the metallic Ag adatom. From previous DFT adsorption study,[28] it has be shown despite numerous trial adsorption sites that ethene molecule binds (0.4 eV) to two types of the surface Ag atoms: one Ag atom from O−Ag−O linkage locating in the center of the dotted hexagon drawn in Figure 1 (1) and one metallic Ag adatom. After a closer look at the oxide registry, two subgroups of oxide-like Ag atoms are present, those sitting directly above one Ag substrate atom (top) and those sitting above three Ag (three-fold). The latter category does not allow stable adsorption. Since metallic Ag sites present no O atom in their vicinity to form an oxametallacycle, one single Ag active site is present on the considered catalyst. Furthermore, STM experiments have corroborated this assumption.[28]

Among the key features of this reactivity study, one should notice the strong modification of the surface-oxide structure during the oxidation process as shown in Figure 1 (1′). The active site has moved in the plane parallel to the surface toward a neighboring metallic Ag atom and forms a dimer bond that further stabilizes the single Ag adatom. In our previous adsorption study,[28] the catalyst flexibility has been already mentioned for the active Ag site which is shifted vertically outward from the mean surface plane. However, this simultaneous lateral shift is a new finding that remains during oxidation processes.

Scheme 1 . Two-Step Oxidation Process on a $Ag^{+\delta}-O-Ag^{+\delta}$ Active Fragment of the Oxide Overlayer[a]

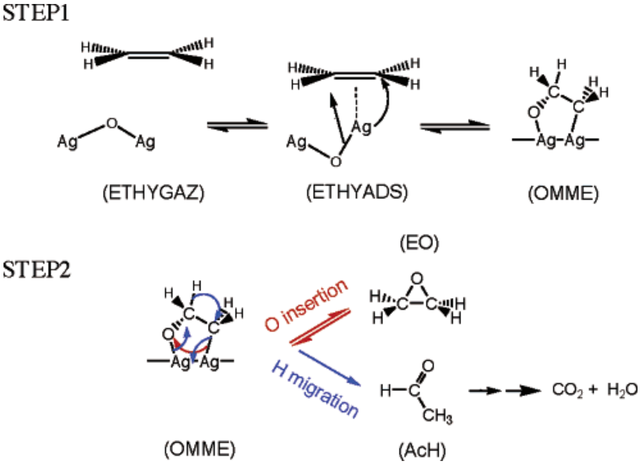

[a] First step is the formation of the OMME (oxygen metal metal ethene) intermediate from an adsorbed ethene precursor (Langmuir−Hinshelwood mechanism). As second step, two outcomes from the OMME structure are possible: along the upper channel, ethene epoxide (EO) is formed through O insertion (step 2a). Along the lower channel, an H-migration between adjacent C atoms leads to an acetaldehyde intermediate (AcH), which will further react to yield CO_2 and H_2O (step 2b).

3.1.2. Reaction Mechanism on Surface-Oxide. As recalled in the Introduction, competitive oxidation processes on this surface-oxide can be inferred similarly to that on clean Ag (see Scheme 1): as two consecutive steps: first sequential routes and second parallel routes.

Since the surface intermediate OMME (OMME recalls for the cycle formed between oxygen−metal−metal−ethene) obviously requires the coordination to two Ag atoms from the catalyst surface, one of the six neighboring Ag atoms to the active site should take part in the reaction mechanism. Because of the resulting OMME structure, this extra Ag atom should also be bonded to the extractable oxygen. In Figure 1 (1) the upper oxygen beside the considered active site (at the center of the unit cell) is indeed three-fold coordinated to Ag surface atoms. The extra Ag atom actually refers to two equivalent Ag surface atoms, but we only represent one for sake of clarity. Thus, it is convenient to reduce our complex catalyst surface to an active Ag−O−Ag fragment as in Scheme 1. The second step accounts for the formation of the second C−O bond with two parallel pathways: either consecutive formations of two single C−O bonds leading to ethene epoxide (EO), or one C═O bond formation giving acetaldehyde (AcH). The further degradation of AcH into carbon dioxide and water has not been examined, since it is known to occur rapidly. All steps (steps 1, 2a (EO), and 2b (AcH)) are completely explored in the present work by means of the NEB approach.

3.1.3. Characterization of Intermediates. Concerning steps 1 and 2a, the NEB procedure enables us to confirm previous transition states and intermediates obtained by constrained minimization technique[16] but interestingly reveals a gallery of analogue states (cf. Figure 2): two molecular precursors for adsorbed ethene (states (2) and (3)) and two conformers (eclipsed (5′) and staggered (5) states) for the OMME intermediate. The main difference between related states is the catalyst structure showing for states (3) and (5) a distorted oxide similar to the state (1′) depicted in Figure 1, whereas states (2)

---

(28) Bocquet, M.-L.; Sautet, P.; Cerda, J.; Carlisle, C. I.; Webb, M.; King, D. A. *J. Am. Chem. Soc.* **2003**, *125*, 3119.

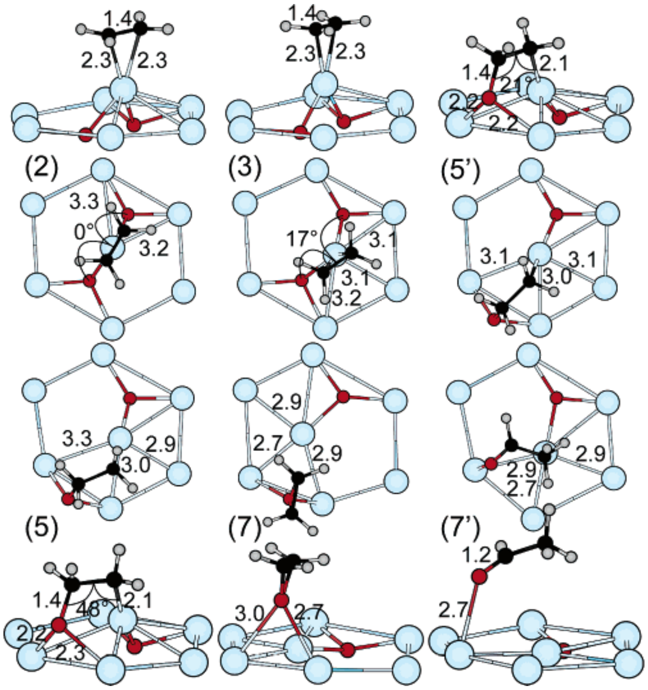

Figure 2. Lateral and top views of intermediate structures: (2) symmetric ethene adsorption state, (3) asymmetric ethene adsorption state, (5′) eclipsed oxamatellacycle, (5) staggered oxametallacycle, (7) EO, (7′) AcH. On these zoomed views the central Ag active site plus its immediate shell of O and Ag atoms are represented (cf. hexagon in Figure 1). Bonding distances are provided in Å. Two molecular precursors have been indeed found along the route toward OMME intermediate: (2) has been already recorded,[16,28] (3) has its C−C axis aligned with one O−Ag bond, the other being bent because of lateral shift of the active site.

and (5′) reveal a symmetric central position for the Ag active site as shown in state (1).

Next, competitive oxidation steps yield adsorbed products EO(ads) (7) and AcH(ads) (7′). For EO(ads) the extracted oxygen is weakly bonded to two Ag atoms in a bridge position, whereas for AcH(ads) the oxygen is only monocoordinated in a top position. Top views in Figure 2 exhibit a similar local reduction of the catalyst beneath EO and AcH, forming a diamond-shaped pattern of four Ag atoms.

To compare the relative stabilities of all presented states, we compute binding energies with reference states being gaseous molecules and either the symmetric surface-oxide (most stable) for reactants or the resulting O-deficient surface-oxide for the products. BE values are respectively −0.22 eV (2), −0.18 eV (3), −0.10 eV (5′), −0.19 eV (5), −0.16 eV (6), −0.10 eV (7), all in the same range showing a constant weak bonding to the surface, which is consistent with feasible reactivity only under high-pressure conditions.

Concerning states (2) and (3), the first symmetric adsorption (2) is the most stable regarding the same reference for the substrate. However, to better quantify the bonding strength in state (3) one should refer to the distorted oxide of which the deformation cost is evaluated at 0.08 eV. Then ethene appears to be slightly more chemisorbed in state (3) in concordance with its precursor position on the pathway. In the energy profile, presented in Figure 3, both adsorbed states are kept, and the precursor state (3) is labeled as a molecular reactive state along the pathway toward OMME.

Concerning OMME formation, the crucial point is that the extractable oxygen has to move from a subsurface four-fold location in precursor state (3) toward an on-surface bridge position in states (5) or (5′). This route looks like a long counterintuitive way to go by analyzing the bare surface-oxide. In fact this catalyst directly offers a number of outmost O atoms and intuitively the gaseous ethene should simply extract such O atom in a concerted mechanism. Despite intensive trials, this obvious scenario has not been validated. We propose on this basis that gaseous ethene experiences repulsive forces in the vicinity of outmost O atoms.

Moving now to the analysis of the key intermediate, two related conformations have been characterized for OMME (see (5) and (5′) in Figure 2). The side views of Figure 2 show that CH_2 groups are almost eclipsed in (5′) and staggered in (5) similar to a Newman projection in conformational analysis. After a closer look at the structures, we infer that the staggered conformation (5) is combined with the substrate deformation. In fact the eclipsed conformer (5′) has a C−C bond perfectly aligned with O and Ag bonded to C (or equivalently C−C lies in the plane containing O and Ag) since the active Ag site remains at its central position. On the other hand, the staggered conformer (5) shows a C−C bond which no longer aligns to the segment linking O and Ag, because of the surface-oxide adjustment. The substrate flexibility hence allows a further opening of the dihedral angle O−C−C−Ag from 21° (“almost” eclipsed) up to 48° (“almost” staggered). From relative binding energies it can be already postulated that the intermediate (5) is the most stable one. Usually a staggered configuration is more stable than an eclipsed one when free rotation around C−C bond is allowed, since it relieves some steric repulsion between substituent groups. Here, despite rigidity imposed by the linkage to the catalyst, the staggered position remains more favorable because of the substrate elasticity. A further accurate vibrational analysis corroborates total energy calculations and actually shows that (5) is a true local minimum, whereas (5′) is a saddle point with one pure imaginary frequency at i190 cm^{-1} (conformational transition state), corresponding to the torsion of the dihedral angle H−C−C−H.

It should be added that staggered OMME structures have been already registered without any specific mention by Linic et al on Cu/Ag alloy surface[29] and by us[16] (discussed next in section 3.2.1). Except for these two cases, OMME intermediates are always proposed as eclipsed conformers. Here, with the help of vibrational characterization, we even rule out the eclipsed form being a saddle point.

3.2. Reaction Pathways. Figure 3 displays zero K energy profiles for the complete catalytic cycle: first, oxidation pathways on the surface-oxide, second, oxidation steps on the O-free surface-oxide and third regeneration pathways on the double O-free surface-oxide. First and third phases arise from intensive NEB calculations, while the second phase is deduced from the first one although the substrate has been locally singly reduced. We later justify this approximation.

3.2.1. Oxidation Pathways. In the first phase of the complete mechanism, gaseous ethene is trapped moderately into two successive chemisorbed states (states (2) and (3) in Figure 3) and then evolves toward the key intermediate OMME (5) with an activation energy barrier of 0.68 eV (step 1). It is found that this first step (step 1) is almost athermic. The second step corresponds to two competing channels: the epoxidation

---

(29) Linic, S.; Jankowiak, J.; Barteau, M. A. *J. Catal.* **2004**, *224*, 489.

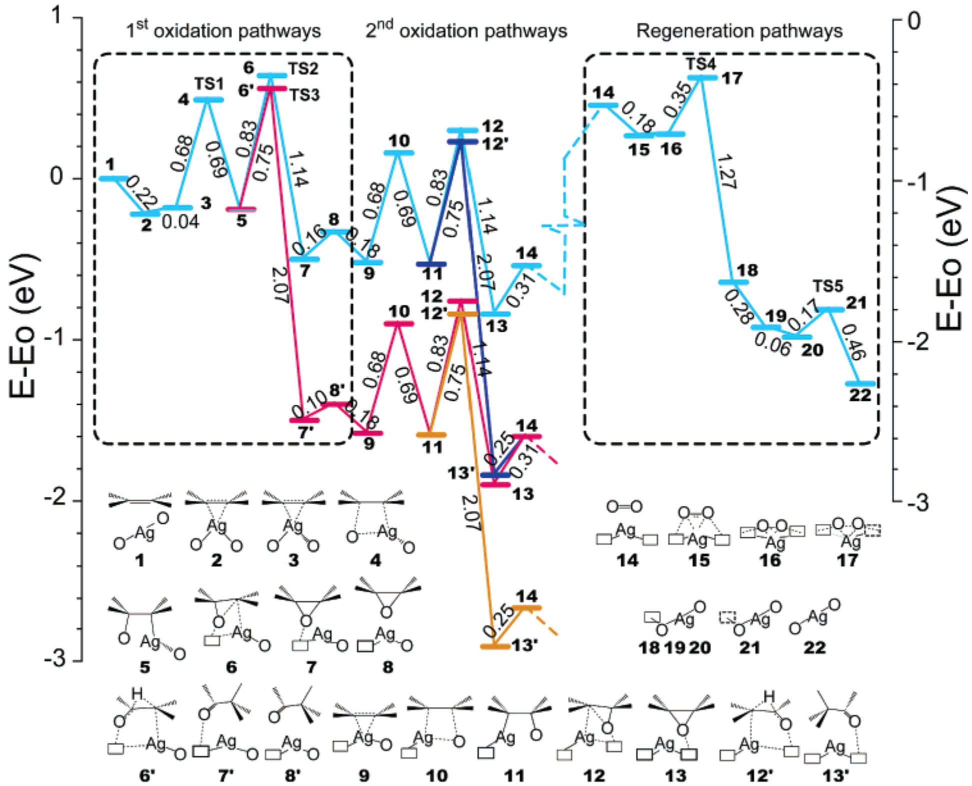

Figure 3. Energy profile for the complete catalytic cycle divided into three phases: (1) ethene oxidation pathways extracting one oxygen from the surface-oxide, (2) ethene oxidation pathways extracting a second oxygen and (3) regeneration pathways with O_2 dissociation and diffusion route to retrieve the initial surface-oxide (they should appear four times starting from state 14). Only MEPs included into large dotted rectangles have been computed with the NEB approach. Second phase is a guessed process exactly similar to first phase. Intermediate and transition states are labeled with consecutive numbers, and their structures are recalled with simple skeletons on the left bottom side. Each labeled state corresponds to two (four) subsets during the first (second) oxidation phase because of competitive thermodynamic versus kinetic processes. Small solid rectangles in the lower scheme panel mark the formation of oxygen vacancies in the oxide substrate during oxidative processes.

reaction (step 2a) with activation energy of 0.83 eV (one imaginary frequency of i195 cm^{-1}) and the isomerization reaction (step 2b) with lower activation energy of 0.75 eV (one imaginary frequency of i1034 cm^{-1}). The total energy difference between steps 2a and 2b corresponds to 1.9 kcal/mol. From previous studies on clean Ag from Linic et al.,[6] only the Gibbs free energy difference is reported and found much lower 0.3 kcal/mol in favor of EO. At this stage direct comparison is not possible since Gibbs free energies have not yet been computed.

However, these sets of energetic results for steps 1 and 2a can be compared with our previous study on both clean Ag and this surface-oxide. We proposed indeed an endothermic step 1 with a higher barrier (0.74 eV) and an exothermic step 2a with a lower barrier (0.74 eV). A quantitative consistency is obtained when considering the new higher-lying state (3) (+0.04 eV) and lower-lying state (5) (−0.09 eV) as initial states for step 1 and step 2a, respectively.[30] Interestingly, optimized structures of the three transition states TS1 (4), TS2 (6), and TS3 (6′) (see Figure 4) shed light into the entire atomic-scale mechanism.

Let's focus on the newly computed step 2b recalled in Figure 5. It belongs to the well-known category of concerted sigmatropic reactions[31] and is based on orbital assistance. In fact, concerted breaking of C1−H1 and C2−Ag(M3) bonds may only happen if they are positioned in *anti* arrangement so that the simultaneous C2−Ag(M3) bond breaking and newly C2−H1 bond forming do perfectly align (see atomic labels in Figure 5). Hence such an orbital-controlled mechanism is expected to be more favorable over our surface-oxide, since the staggered OMME intermediate already offers such favorable disposition. As shown in Figure 4, the TS3 structure (6′) presents one C−H bond breaking (distance 1.2 Å), and one C−H bond forming (distance 1.5 Å) and is comparable to the structure found on clean Ag by Linic et al. In addition the computed imaginary mode for TS3 is a high-frequency mode at i1034 cm^{-1}

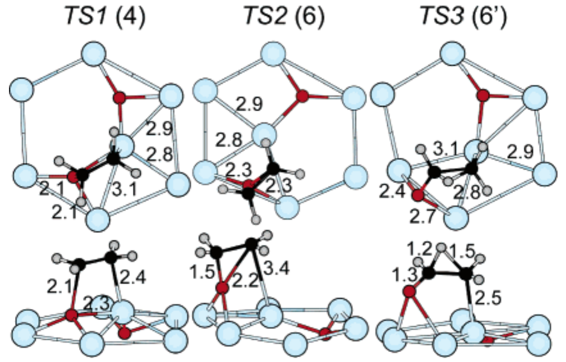

Figure 4. Different top and lateral views of TS1 (4), TS2 (6), and TS3 (6′) with some key distances. On all top views, the in-plane shift of the central active Ag site assesses for the constant deformation of the surface-oxide during the oxidation reaction.

---

[30] To avoid any confusion, we mention that the staggered OMME structure accompanying the pathway of ref 16 does not correspond to the reported energy. The corresponding fine optimization was not fully satisfactory at that time, and we anticipated its final structure.

[31] Carey, F. A.; Sundberg, R. J. *Advanced Organic Chemistry*, Part A, 3rd ed.; Plenum Press: New York, 1990.

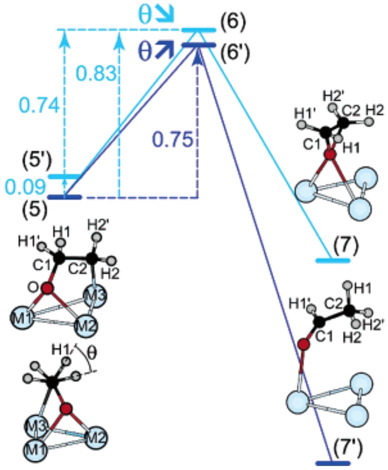

Figure 5. Energy profile snapshot of two parallel oxidation steps starting from the staggered OMME (5) represented by the dihedral angle θ. On the lower lateral view of state 5, H1 atom bisects the plane formed by the next H2−C2−H2′, and the C1−H1 bond is precisely in *anti* configuration relative to C2−Ag M3 atom. Barrier decomposition reveals that the additional energetic cost for step 2b ((5) to (7)) compared to step 2a ((5) to (7′)) exactly corresponds to the conformational barrier ((5) to (5′)) of the OMME intermediate.

corresponding to the jump of the H atom between adjacent carbon atoms. As for step 2a, the reaction coordinate first undergoes a conformational inversion since three-membered ring closure is a *syn* mechanism. Moreover, the very loose C−O bond in TS2 being 2.2 Å is fully consistent with a low-energy imaginary mode at i195 cm^{-1} assigned to weak C−O stretch. To summarize, the preferential OMME staggered conformation is mandatory for the AcH concerted formation. Conversely the EO formation comes from the higher-energy eclipsed conformer. As shown in Figure 5 zero K energy difference between TS2 and TS3 (0.08 eV) can be totally attributed to the torsion cost of the dihedral angle H−C−C−H. This barrier decomposition supports the idea that both formations of the second C−O bond (steps 2a and 2b) have similar intrinsic barriers, but they originate from different conformations of the surface intermediate. On our flexible catalyst, the stable, staggered conformation does exist as a true local minimum, and consequently our catalyst is shown to favor the isomerization.

Last, the second section of Figure 3, referred as to the second oxidation phase, has been assumed to occur similarly despite a local metallization of the surface. Precisely the starting assumption prior to ethene reactivity concerned an exclusive occupation of one single type of Ag active sites on this surface-oxide as already discussed before. Such preferential sites are still available in the reduced surface and still prevail before newly formed metallic sites since ethene does not stick to clean Ag surfaces within our DFT approach.[16] Then one may count on the singly reduced surface two similar sites at the edges of the 4 × 4 unit cell, which lead equivalently to the most stable arrangement for the doubly reduced oxide as shown later in Figure 6 (state (14)). In fact, it corresponds to the extraction of two adjacent oxygens within the same oxide ring.[32] On this basis, we assume that successive extractions of O atoms occur the same way.[33] Because of the competing channels we have therefore four routes after this second oxidation process with different mixtures of products.

3.2.2. Regeneration Pathways. After two oxidation cycles, the catalyst is left with two oxygen vacancies. As represented in Figure 6, the resulting doubly reduced oxide (14) displays two triangular patterns of metallic Ag atoms connected through one apex Ag1. Among few trial molecular precursor states for O_2 dissociation reaction, we found the most stable adsorption state (state (15) in Figure 6), where both oxygen atoms (labeled α and β) are nearly bridge (to Ag4−Ag1)−nearly bridge (to Ag1−Ag3) bonded. This so-called *exo* molecular configuration evolves first into a related *endo* state (16) after a large lateral shift of Ag1: the diamond-shaped pattern formed by Ag1−2−3−4 atoms has transformed into a square cluster, enabling the oxygen molecule to lie in plane of Ag atoms and to be fourfold coordinated. Precisely, Oβ is lying in the Ag plane, but Oα remains on the surface. This new *endo* molecular state revealed by the NEB approach is a straightforward precursor of the dissociation (TS4) as depicted in Figure 6 with elongated distances between oxygen atoms.

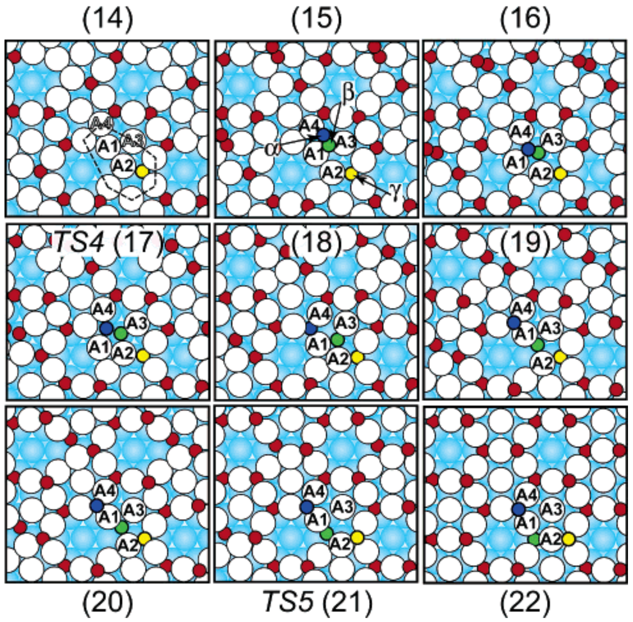

Figure 6. Top views of all stable intermediates found along the oxide-catalyst regeneration pathways. The O atoms appear with small red balls but the three O atoms involved in the regeneration mechanism are shown in small dark blue, green, and yellow balls and noted respectively Oα, Oβ, and Oγ. The surface-oxide Ag atoms are depicted with large white balls, and the underlying Ag substrate atoms are in large blue balls. The four Ag atoms that play a major role are labeled from A1 to A4. In (14) the polygon drawn with black dotted lines defines the neighboring Ag atoms involved in the mechanism. All labeling numbers are the same as in Figure 3: (14) bi-reduced bare surface-oxide prior to O_2 adsorption, (15) most stable O_2 *exo* molecular adsorption state, (16) metastable O_2 *endo* molecular adsorption state, (17) O_2 dissociation transition state TS4, (18) first $2O_{ads}$ metastable dissociated state, (19) second $2O_{ads}$ metastable dissociated state, (20) $2O_{ads}$ stable dissociated state, (21) subsurface Oβ diffusion transition state TS5, (22) symmetric surface-oxide equals to state (1) shown in Figure 1.

From this TS4 structure, the system transforms into several successive dissociated states ((18), (19) and (20) in Figure 6) involving displacements of three labeled O atoms: in the first atomic state, Oα, Oβ, and Oγ are all in subsurface location. In the second state Oα moves to an on-surface location while the two others remain subsurface, and in the third atomic state Oα

---

[32] Bocquet, M.-L.; Michaelides, A.; Sautet, P.; King, D. A. *Phys. Rev. B* **2003**, *68*, 075413.

[33] Our assumption is justified on the basis of complementary calculations devoted to the first step of the second oxidation pathways (corresponding to step (9) → (11) and TS structure (10)). The NEB approach shows a completely consistent activation barrier and TS structure compared to step (3) → (5) (the activation barrier difference being 0.02 eV).

and Oγ lie on the surface, but Oβ still lies subsurface. The next step simply reflects an internal diffusion for Oβ between two tetrahedral subsurface states, the second TS5 structure (21) representing an intermediate situation along the diffusion path where Oβ−Ag3 bond breaks while links to Ag1 and Ag2 remain.

This two-step regeneration pathway reveals very subtle features since it involves one additional O atom in a neighboring subsurface location. First O_2 dissociates after having optimized its coordination to the metallic cluster (four-fold). Next, vertical and lateral moves of O atoms are associated with subsurface diffusion between neighboring tetrahedral sites to regenerate the initial symmetric surface-oxide. The first dissociating barrier is then found to be very low (0.35 eV) compared to that computed by us on clean Ag (0.64 eV)[16] and again results from the easy deformation of the metallic four-member cluster on which O_2 adsorbs. This first step is also the rate-limiting process of the regeneration procedure. From our computed mechanism, we see that Ag1 can easily be shifted toward the vacancy area and then can provide enough space to accommodate the oxygen molecule into an elongated square formed by Ag1 to Ag4 atoms. This vacancy area structurally arises from the assumed Ag deficiency for the surface-oxide[14] compared to bulk oxide stoichiometry. It is possible that the filling of these vacancy areas could prevent such a facile oxygen intrusion to occur. This scenario may be specific to the considered Ag-deficient oxide structure.

In conclusion, subsequent exposure to O_2 thus may restore the original surface structure in a quite rapid way compared to the oxidation procedure, and this step should not be rate-determining as justified in the next kinetic section.

4. Microkinetic Modeling

Once oxidation and regeneration pathways are computed at the atomic scale, the macroscopic activity and the selectivity of the surface-oxide catalyst can be further studied with a microkinetic model, where all rate constants are derived from the total energy calculations. Previously, several approaches have been reported to study the pure Ag surface activity and selectivity toward oxidation.[17,19] The kinetic models are based on a mean-field theory, which has been developed several times in the literature.[34−36] The parameters are usually calculated using statistical thermodynamics for gas-phase molecules and adsorbates.[19] According to previous theory, the steady-state approximation (SSA) is applied to all surface intermediates, equating the corresponding apparition rates to zero. In the proposed formalism, the rate constants are calculated using either the collision theory or the transition state theory.[37]

The microkinetic approach applied here is based on the following fundamental assumptions:

(1) surface elementary steps follow Langmuir−Hinshelwood-type mechanisms (bimolecular or unimolecular event) and satisfy microreversibility;

(2) only two surface sites have been considered despite the occurrence of three substrates in the catalytic cycle: first and second oxidation pathways are considered to occur on a unique active Ag site. The second surface site is on the doubly reduced surface-oxide during the regeneration process;

Table 1. Elementary Steps Occurring in the Oxidation Mechanism (complete cycle of Figure 3) and Considered in the Microkinetic Model[a]

C_2H_4(gas)+[AgO_2 or AgO-□] ↔ C_2H_4(ads)	(step A1)
C_2H_4(ads) ↔ OMME	(step S1)
OMME ↔ EO(ads)	(step S2)
OMME ↔ AcH(ads)	(step S3)
EO(ads) ↔ EO(gas) + [AgO-□]	(step D1)
AcH(ads) ↔ AcH(gas) + [AgO-□]	(step D2)
EO(ads) ↔ EO(gas) + [Ag$□_2$]	(step D1′)
AcH(ads) ↔ AcH(gas) + [Ag$□_2$]	(step D2′)
O_2(gas) + [Ag$□_2$] ↔ O_2(ads)	(step A2)
O_2(ads) ↔ [AgO_2]	(step S4)

[a] (A1), (A2), (D1) and (D2) are the adsorption−desorption steps of ethene and O_2 reactants, EO and AcH products (singly reduced surface-oxide). (D1′) and (D2′) are the same steps for a doubly reduced surface-oxide. From (S1) to (S4), surface elementary steps of oxidation and regeneration pathways.

(3) each surface intermediate occupies only one site;

(4) transition-state theory formulation is applied systematically for the calculation of the rate constants (adsorption, desorption, and surface elementary steps):[38−39]

$$k_i(T) = k_i^0\, \mathrm{e}^{-E_i^{\mathrm{ACT}}/kT} = \frac{kT}{h}\,\frac{Q_i^{\mathrm{TS}}}{\prod_j Q_j^{\mathrm{IS}}}\,\mathrm{e}^{-E_i^{\mathrm{ACT}}/kT}$$

where, for an elementary step i, Q_i^{TS} and Q_j^{IS} are respectively the total partition functions of transition state (TS) and of each intermediate j at the initial state (IS). E_i^{ACT} is the DFT activation energy. The vibrational partition function contributions in all the rate constants are neglected. For steps S2 and S3, we have calculated them and found a correction factor of 30 for k_i^0(S2) and 100 for k_i^0(S3). Zero-point energy variation corrections are −50 meV for S2 and −150 meV for S3, hence giving a negligible net corrective factor in the rate constants of 10 and 5 for S2 and S3, respectively. The translational Q_j^{TRS} and rotational Q_j^{ROT} partition function contributions of each gas-phase compound (ethene, O_2, EO, and AcH) are, however, systematically calculated for adsorption processes;

(5) adsorption−desorption steps are considered as fast events, and the quasi-equilibrium approximation is applied (QEA) at the initial time of the simulation. Only adsorption is considered as nonactivated ($E_{act} = 0$), and the sticking coefficients of all gas reactants and products are equal to 1;

(6) surface steps are all considered as slow events, and corresponding rates are integrated with time using a Runge−Kutta integration scheme. Hence, no SSA assumption is made for the surface reaction intermediates. Surface intermediate diffusion processes are neglected;

(7) reactant partial pressures are constant, and kinetics follow a regime which is not limited by the reactant influx.

In our model, the considered elementary steps are those reported in Table 1. In our notations, θ is the coverage of free

---

(34) Dumesic, J. A. *J. Catal.* **1999**, *185*, 496.
(35) Campbell, C. T. *Top. Catal.* **1994**, *1*, 353.
(36) Lynggaard, H.; Andreasen, A.; Stegelmann, C.; Stoltze, P. *Prog. Surf. Sci.* **2004**, *77*, 71.
(37) Gokhale, A. A.; Kandoi, S.; Greeley, J. P.; Mavrikakis, M.; Dumesic J. A. *Chem. Eng. Sci.* **2004**, *59*, 4679.
(38) Laidler, K. J. *Chemical Kinetics*, 3rd ed.; Harper Collins Publishers: New York, 1987.
(39) van Santen, R. A.; Niemantsverdriet, J. W. *Chemical Kinetics and Catalysis*; Plenum Press: New York, 1995.

Table 2. Rate Equations for the Kinetic Model Based on the Reaction Mechanism Reported in Table 1

$$\partial\theta_2/\partial t = 3(k_{S1}\theta_1 - k_{S-1}\theta_2 + k_{S-2}\theta_3 - k_{S2}\theta_2 + k_{S-3}\theta_4 - k_{S3}\theta_2) \quad (1)$$

$$\partial\theta_3/\partial t = 3(k_{S2}\theta_2 - k_{S-2}\theta_3) \quad (2)$$

$$\partial\theta_4/\partial t = 3(k_{S3}\theta_2 - k_{S-3}\theta_4) \quad (3)$$

$$\partial\theta_5/\partial t = 4(k_{S-4}\theta - k_{S4}\theta_5) \quad (4)$$

Table 3. Forward (*i*) and Backward (−*i*) Rate Constants for Elementary Steps of the Microkinetic Model Calculated at 600 K and with Equivalent Partial Pressures 1 atm of Ethene and O_2 Reactants; DFT Activation Energies (kJ·mol^{-1}) of the Corresponding Forward and Backward Elementary Steps

	E^{act}_i (kJ·mol^{-1})	k_i (600 K)	E^{act}_{-i} (kJ·mol^{-1})	k_{-i} (600 K)
A1	0	4×10^{-24} m^3·s^{-1}	21	2×10^{11} s^{-1}
A2	0	2×10^{-22} m^3·s^{-1}	17	4×10^{11} s^{-1}
D1	0	5×10^{-25} m^3·s^{-1}	15	6×10^{11} s^{-1}
D1′	0	5×10^{-25} m^3·s^{-1}	30	3×10^{10} s^{-1}
D2	0	4×10^{-25} m^3·s^{-1}	10	2×10^{12} s^{-1}
D2′	0	4×10^{-25} m^3·s^{-1}	24	1×10^{11} s^{-1}
S1	69	1×10^{7} s^{-1}	67	2×10^{7} s^{-1}
S2	80	1×10^{6} s^{-1}	110	3×10^{3} s^{-1}
S3	72	6×10^{6} s^{-1}	200	5×10^{-5} s^{-1}
S4	34	1×10^{10} s^{-1}	183	1×10^{-3} s^{-1}

active sites (the same for nonreduced and singly reduced surface-oxide), θ' corresponds to the coverage of the free active sites on the bi-reduced surface-oxide, θ_i (i ranging from 1 to 5) accounts for the coverage of the respective adsorbed species over nonreduced [AgO_2] or singly reduced [AgO-□] surface-oxides: (1) C_2H_4(ads), (2) OMME, (3) EO(ads), (4) AcH(ads), (5) O_2(ads). The partial pressures of the products EO(gas) and AcH(gas) are noted respectively P_{EO} and P_{AcH}.

For fast events (adsorption−desorption processes), the quasi-equilibrium approximation (QEA) is applied.[36] Hence, using the mass conservation balance $\sum\theta_i = 1$, the coverage of free active sites θ can be expressed as a function of surface species coverages θ_i (i ranging from 2 to 4):

$$\theta = \frac{1 - \theta_2 - \theta_3 - \theta_4}{1 + \dfrac{k_{A1}}{k_{-A1}} P_{C2H4} + \dfrac{k_{-D1}\, k_{D1'}}{k_{D1}\, k_{-D1'}}\left(1 + \dfrac{k_{A2}}{k_{-A2}} P_{O2}\right)}$$

The set of the net rates reported in Table 2 can then be integrated using a Runge−Kutta integration scheme. In this scheme, the maximum integration time is 10^{-4} s. These rates account for all the elementary steps presented in the complete catalytic cycle (Figure 3), hence justifying the apparition of a factor of 3 in eqs 1−3 or a factor of 4 in eq 4.

Parameters of the model are given in Table 3 for a temperature of 600 K. The activation energies of desorption processes and the surface elementary steps (forward and backward S2, S3, backward S1 and forward step S4) are those reported previously in Figure 3. For the forward step S1, the activation energy includes the diffusion energy between the two ethene adsorption sites (0.04 eV cf. Figure 3). For the backward step S4, the activation energy is summed over all the intermediate states between TS4 (17) and the final retrieved surface-oxide (22) (see Figure 3 for the notations).

Our kinetic parameters are similar in order of magnitude with those published previously by Linic et al.[17] when equivalent units are used. For the purpose of consistency, we apply the transition state theory also for the adsorption process conversely with previous works where the collision theory is used.

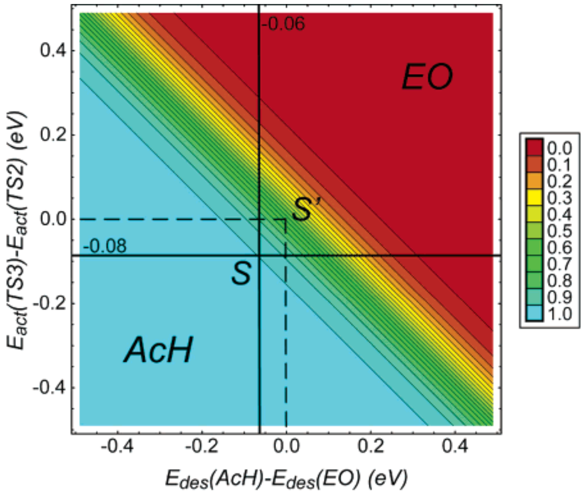

Figure 7. Contour plot of the selectivity of AcH (ranging from 0 to 1) as a function of the desorption energy difference (eV) between the competitive products ethene epoxide (EO) and acetaldehyde (AcH), and the activation energy difference between the elementary steps S2 and S3 associated with the transition states TS2 and TS3, respectively. The temperature is set to 600 K, and the partial pressures of ethene and O_2 are equivalent (1 atm). When E_{act}(TS3) and E_{des}(AcH) are set to the DFT calculated values (see Figure 3), the energy differences ΔE_{act} and ΔE_{des} are respectively −0.08 and −0.06 eV, and the selectivity is 96% in favor of AcH (point S). For identical values of both desorption and the activation energies, the selectivity in AcH rapidly decreases to 66% (point S′).

At 600 K and equivalent partial pressures of 1 atm for both reactants ethene and O_2, the product obtained selectively is AcH (96%), in contrast with classical metallic Ag surfaces (40%)[6] and experiments (20−50%[40]). The turnover frequency (TOF), which is the net rate of AcH in our case, is independent of the partial pressure of oxygen since the oxygen regeneration elementary steps only appear at the final stage of the microkinetic model. The apparent activation energy of the overall reaction is calculated classically by plotting the TOF as a function of the temperature.[19] In the temperature range 550−750 K, the correlation is perfectly linear, and the calculated apparent activation energy (9 kcal·mol^{-1}) does not depend on the ethene partial pressure. This value is slightly lower than the experimental and theoretical results published previously.[17] The calculated TOF (10^{-2}−10^{-4} s^{-1}) shows that the silver oxide surface is slightly less efficient than classical silver catalysts.[19]

Another important kinetic descriptor is the selectivity of AcH which is defined in our model as [AcH(gas)]/{[AcH(gas)] + [EO(gas)]}. The surface-oxide catalyst offers 96% selectivity in favor of AcH, with a negligible dependence on the initial conditions of temperature and pressure. Because of the discrepancy with previous results on pure Ag catalysts,[6] the sensitivity of such a descriptor has been checked by changing continuously two controlled parameters of the model: the energy difference between the activation barriers responsible for the competitive pathways (TS2 and TS3) and between the desorption energies of competitive products (EO and AcH). As shown in Figure 7, the natural AcH selectivity (96% referenced with S) strongly depends on both energetic perturbations.

---

(40) Kestenbaum, H.; de-Oliveira, A. L.; Schmidt, W.; Schuth, F.; Ehrfeld, W.; Gebauer, K.; Lowe, H.; Richter, T.; Lebiedz, D.; Untiedt, I.; Zuchner, H. *Ind. Eng. Chem. Res.* **2002**, *41*, 710.

As shown in Figure 7, if the activation barriers leading to TS2 and TS3 and the desorption energies of EO and AcH were identical, the catalyst would offer a much higher selectivity in favor of EO (66% of AcH referenced with S′). Hence, a small perturbation of ΔE_{act} and ΔE_{des} (60−80 meV) can completely change the calculated selectivity. The high sensitivity of this kinetic parameter thus requires very accurate DFT calculations. To ensure a thorough prediction of selectivity, systematic and numeric errors intrinsically linked to the choice of the model (supercell, GGA functional) should be evaluated very carefully. At least the activation energy should include vibrational entropic contributions systematically, which is not an easy task for large periodic systems.

As a last checking, the convergence of ΔE_{act} and ΔE_{des} has been investigated by changing input parameters such as k-point density or by changing the model with different pseudopotentials (PAW) set. The error bar is found lower than 20 meV. This validates quantitatively our energetic results but does not reverse the predicted trend for selectivity. Next, following Linic and co-workers' approach, total energies have been replaced in the kinetic model by free energies ΔG_{act} and ΔG_{des}. Entropic contributions (zero-point energy corrections and vibrational partition function contributions) have been determined with the calculated vibrational modes for the staggered OMME, TS2, and TS3. As a result ΔG_{act} is even more in favor of AcH with −0.18 eV since ZPE for TS2 is +0.1 eV higher than ZPE for TS3. These computed results strengthen the definitive reverse selectivity to AcH even when entropic contributions are taken into account. However, it should be pointed out that the proposed link between ab initio energy difference between activation energies and selectivity has to be regarded with caution since a little perturbation of the order of a 60−80 meV may alter the picture for the resulting selectivity.

5. Conclusion

Elementary steps of ethene epoxidation, acetaldehyde isomerization, and surface-oxide regeneration have been determined using DFT slab calculations on a p(4 × 4) surface-oxide adlayer on Ag(111), starting with a specific active Ag site from O−Ag−O linkages. At first sight, a similar branching route is retrieved to produce EO and AcH species starting from the same oxametallacycle intermediate. On one hand, our results corroborate the evidence for a pivotal intermediate in selective epoxidation on various Ag−O local environments. To date, this branching mechanism originally proposed by Linic et al. for ethene on clean Ag catalyst has been only generalized to higher olefins such as butadiene[41] and styrene.[42] On the other hand, our mechanism displays two reverse features, which are assigned to the smoothness of the surface-oxide catalyst: a staggered conformation of the oxametallacycle and an activation energy preference for the nondesired intermediate.

Eventually, we propose a correlation between both findings that sheds light into the origin of the selectivity. We point out that the ring closure toward the epoxide requires a *syn* arrangement or equivalently an eclipsed OMME conformation, whereas the staggered OMME conformation facilitates the H migration in an *anti* orbital-assisted process. By further postulating equal intrinsic energy barriers for both C−O bond formations when starting from their reactant conformations, the difference in activation energies may only result from the conformational barrier of the oxametallacycle.

To be able to compare our mechanistic approach with kinetic measurements, a microkinetic model is developed to compute the selectivity. We find 96% selectivity in favor of AcH and demonstrate that this observable is mainly tuned by two crucial relative energies: activation energies difference between competitive steps and desorption energies difference between competitive products. As expected with low computed barriers for oxide regeneration, O_2 dissociation is not a determining step as it is on clean Ag.[17] Despite a high sensitivity to DFT values, systematic errors and entropic corrections are not able to reverse the proposed trend. Last, DFT and microkinetic results naturally question the relevance of this high oxygen coverage surface as a realistic epoxidation catalyst. According to the present study, the pure silver domains of the dual-phase catalyst stable in realistic conditions seem to offer a higher activity and selectivity toward ethene epoxidation than the considered surface-oxide phase.

Acknowledgment. We thank P. Fleurat-Lessard and A. Michaelides for valuable discussions and IDRIS (CNRS, France) for CPU time and assistance (project 609).

Supporting Information Available: Geometries of intermediates and transition states for the multiple-step regeneration pathways. This material is available free of charge via the Internet at http://pubs.acs.org.

JA051397F

---

(41) Barteau, M. A. *Top. Catal.* **2003**, *22*, 3.
(42) Enever, M.; Linic, S.; Ufalussy, K.; Vohs, J. M.; Barteau, M. A. *J. Phys. Chem. B* **2005**, *109*, 2227.